Results in Physics 10 (2018) 411–423

Contents lists available at ScienceDirect

Results in Physics

journal homepage: www.elsevier.com/locate/rinp

An acoustic modeling of the three-dimensional annular segment cavity with various impedance boundary conditions

Yujie Xiao[a], Dong Shao[a,b], Hong Zhang[c], Cijun Shuai[d], Qingshan Wang[d,*]

[a] Naval Research Academy, Beijing 100161, PR China
[b] Beijing Aerospace Technology Institute, China Aerospace Science & Industry Corp., Beijing 100074, PR China
[c] College of Mechanical and Electrical Engineering, Harbin Engineering University, Harbin 150001, PR China
[d] State Key Laboratory of High Performance Complex Manufacturing, Central South University, Changsha 410083, PR China

ARTICLE INFO

Keywords:
Fourier series
Annular segment cavity
Impedance wall
Rayleigh-Ritz technique

ABSTRACT

A three-dimensional Fourier series method (3D-FSM) is applied to study the acoustic characteristics of annular segment acoustic cavity with various impedance boundary conditions. The formulation is constructed to describe the cavity system based on the energy principle. Under the framework of this paper, the admissible sound pressure function is generally set, regardless of boundary conditions, to a 3D Fourier cosine series and six supplementary functions. These supplementary functions can eliminate the discontinuous or jumping phenomenon in the boundaries. All the series expansion coefficients can be obtained through the Rayleigh-Ritz technique. The results obtained by the present method in this paper show good convergence. The accuracy of the present method is verified by being compared with the exact solution and the finite element method (FEM). The natural frequencies and modal shapes of the annular segment cavity are studied. The sound pressure response is investigated under the excitation of a monopole source inside the cavity. In this paper, some results of the acoustic characteristics of the cavity with various geometric parameters and boundary conditions are obtained, such as angle, radius ratio, impedance value and the number of impedance wall. These results provide a benchmark for the future researches.

Introduction

As the basic structure, the annular segment cavity is widely used in engineering application, such as aerospace, marine engineering, civil construction, rockets and rail transportation. Therefore, there is important applicative value for the study on annular segment cavity system and cylindrical cavity system which is of great significance in the acoustic design and noise control of complex acoustic space. So far, the study on acoustic properties of enclosed space has been well-rounded. These results provide an important theoretical basis for the further research. But, there are some limitations in the study on the varying impedance boundary conditions. Therefore, this paper aims to study the acoustic characteristics of annular segment cavity with various impedance boundary conditions.

The rectangular cavities, as the simplified model of room acoustics, have been extensively investigated. There have been many research results on acoustic characteristics of the two-dimensional (2D) rectangular cavities with rigid-wall and impedance-wall boundary conditions, which have built a good fundament for the future research. Koch [1] computed numerically in 2D rectangular deep and shallow open cavity. Huang and Jiang [2] discussed the circular line sound source model for 2D thin acoustic cavity by using the transfer matrix method. This model avoided the singularity of source and obtained the uniform pressure responses on the circular line. Dhandole and Modak [3] extended the sequential quadratic programming algorithm to solve the constrained optimization problem, which is used to update the acoustic finite element model. The sound pressure responses of a 2D rectangular cavity and a car cavity were verified based on this method. González et al. [4] used spectral element spatial discretization to analyze the acoustic resonances of a 2D open cavity with absorbing boundary conditions by solving a multi-dimensional Helmholtz equation. Aktas et al. [5] considered the Navier-Stokes equations to simulate a 2D rectangular enclosure filled by compressible gas. The frequencies were considered along the enclosure in which the oscillatory flow field is created through the vibration of the left wall of the enclosure.

With the gradual deepening of the research, the study on the acoustic characteristics of the 3D rectangular cavity or rectangular-like cavity model has attracted wide attention. Huang and Jiang [6] extended Ewald's summation technique to calculate acoustic Green's function for closed rectangular cavity. This transformed Green's

* Corresponding author.
E-mail address: qingshanwang@csu.edu.cn (Q. Wang).

https://doi.org/10.1016/j.rinp.2018.06.039
Received 25 April 2018; Received in revised form 30 May 2018; Accepted 18 June 2018
Available online 22 June 2018

function showed fast convergence. Larbi et al. [7] applied a new finite element formulation to study the internal acoustic problems with absorbing walls by introducing the normal fluid displacement field on the damped walls. Pàmies et al. [8] investigated the sound radiation from an aperture in a rectangular enclosure under low modal conditions by using the Rayleigh radiation equation. Li and Cheng [9,10] investigated acoustic modes of a rectangular-like cavity with a slight geometrical distortion introduced by a leaning wall. Petyt et al. [11] developed an isoparametric acoustic finite element model with twenty nodes, which was first used to study the rectangular enclosure. Petyt et al. [12] obtained some results of the rectangular cavity containing a rigid and incomplete partition by using FEM. Pan et al. [13] introduced the modal expansion approach to study the sound pressure response of rectangular enclosures which had suitable modification of the damping and frequency shift on the rigid-wall. The Helmholtz resonance effects of the cockpit in a helicopter were also considered in the model. Nabavi et al. [14] reported an experimental analysis of the non-linear phenomena of regular and irregular acoustic streaming patterns which were in a square air-filled channel with rigid-wall based on the synchronized particle image velocimetry technique. Guha et al. [15] presented a partly flexible laminated composite enclosure based on finite element free vibration analysis and boundary element solver. Du et al. [16] studied the acoustic characteristics of the rectangular cavity with general impedance boundary conditions. A variety of boundary conditions of rectangular cavity are studied, including rigid wall, impedance wall and fully absorbing wall. A lot of existing researches are made on the rectangular and rectangular-like cavity, but the studies on other shape cavities are rare. Shi et al. [17] proposed an analytical to study the vibro-acoustic behaviors of a double-plate structure with an acoustic cavity. In this model, two dimensional (2D) and three dimensional (3D) modified Fourier series were used to represent the displacement of the panels and the sound pressure inside the cavity. Applying the modified variational method, Xie et al. [18,19] studied the acoustic properties and vibro-acoustic responses of irregular enclosures. The Chebyshev polynomial exhibits high performance at entire field approximations. Bouillard et al. [20] developed an improved element-free Galerkin method for the acoustic problem of three-dimensional complex geometries. Bouzouane et al. [21] investigated the ultra-thin films effects on vibro-acoustic behavior of a laminated glass plate composed of two elastic skins, a viscoelastic core and two ultra-thin adhesive films based on the classical plate's theories. Following the energy method, Zhang et al. established a composite thin plate-cavity coupling system [22] based on CPT and the moderately thick laminated rectangular plate-cavity coupling system [23] based on FSDT. Shi et al. [24] presented a general solution method to predict the dynamic behaviors of the three-dimensional (3D) acoustic coupled system of a partially opened cavity coupled with a flexible plate and an exterior field of semi-infinite size. Later, Shi et al. [25] extended this solution to further study the modeling and acoustic eigenanalysis of coupled spaces with a coupling aperture of variable size.

In real-world applications, there are many cylindrical acoustic cavities, such as rocket, submarine, aircraft cabin and so on. The existing literature researches for rotary-shaped annular segment cavities and cylindrical cavities have obvious limitations. Laulagnet et al. [26] used modal analysis to study acoustic radiation of finite cylindrical shell which was immersed in heavy fluid. In this paper, the related concepts of radiation and damped modes were introduced. In addition, this study also gave an important discovery that the behavior of a shell in water is very different from that of one in air. Gardonio et al. [27] investigated the plane wave transmission characteristic of a circular cylindrical sandwich-shell based on the modal interaction analysis. The model established in this paper can be used to study the high order acoustic modes and investigate the sensitivity to damp and cavity absorption. Yang et al. [28] used an integro-modal approach to deal with sound radiation from a finite cylindrical shell with an irregular-shaped acoustic enclosure. The cylindrical shell contains a machinery equipment modelled as a rectangular object attached to shell with a spring-mass system. In addition, effects of the object size on the coupling between acoustic modes and structural modes were investigated. Shi et al. [29] proposed the acoustic radiation force function on a solid elastic spherical particle placed in an infinite rigid cylindrical cavity filled with an ideal fluid. It is not difficult to find that there are few studies on the annular segment cavity or cylindrical cavity with various impedance boundary conditions.

Considering the restrictions of the rotary-shaped cavity with various impedance walls in the current researches, the acoustic characteristic analyses of the annular segment cavity with rigid-wall and various impedance-wall boundary conditions are developed. Based on the Rayleigh-Ritz energy technique, a 3D Fourier series solution is extended to study the sound properties of annular segment cavity with various impedance boundary conditions. This method is previously proposed by Du et al. [16] to study the rectangular cavity with general impedance boundary conditions. The sound pressure functions can be written as a feasible superposition of the 3D trigonometric series expansion, ignoring the effect of boundary conditions, in spectral form, as a 3D Fourier cosine series and six supplementary functions. On the basis of traditional Fourier series, these supplementary functions are added to eliminate the discontinuous or jumping phenomenon in the boundaries which are regarded as a periodic function and defined within the entire coordinates of the cavity. All these unknown coefficients are defined in the generalized coordinates which can be solved by Rayleigh-Ritz procedure. In our previous work [30–41], this kind of Fourier series method has been used to investigate the vibration characteristics of 2D solid structures. The results obtained by the present method are compared with those results obtained by literatures and FEM, which shows good agreement. The current work mainly deals with the natural frequencies, mode shapes, and sound pressure responses with significant constraints such as arbitrary sector angle, geometric dimension and various values of impedance parameters. These parametric studies have guiding significance for the acoustic noise control of annular segment cavity.

Theoretical formulations

Description of the model

As shown in Fig. 1, an annular segment cavity model is established to analyze characteristics of the three-dimensional sound field. For the annular segment cavity, the dimensions of the cavity with general wall impedance are listed here: outer radius, inner radius, height and sector angle dimensions are R_1, R_2, h and ϕ, respectively. An integral cylindrical coordinate system (O-$r\ \theta\ z$) and a local-coordinate system (O'-$s\ \theta\ z$) in the cavity model are established. In local-coordinate system, s represents the difference between the outer radius and the inner radius which is expressed as R_1-R_2. Besides, θ and z represent the angle and height directions of the studied model. A monopole source Q is located at a corner of the annular segment cavity.

Admissible sound pressure functions

The modal characteristics of annular segment closed space under various impedance boundaries can be obtained by solving 3D homogeneous Helmholtz acoustic equation and the boundary value problem of the impedance acoustic boundary constraint equation. It is assumed that the distribution of impedance on the wall is same and the attenuation effect of medium viscosity is ignored in sound propagation process. Under this condition, the boundary value problem can be described as:

$$\frac{\partial p}{\partial n} = -j\frac{\rho c_0}{Z_i}kp \tag{1}$$

where p, c_0 and ρ are the acoustic pressure, the speed of sound

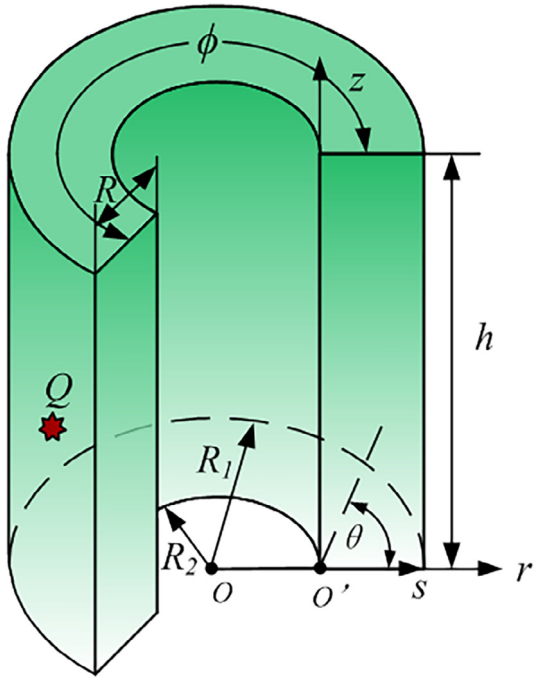

Fig. 1. The annular segment cavity with acoustical impedance boundary.

propagation and the mass density of the acoustic medium, respectively. Moreover, n is the outer normal direction of the enclosure surface, j is the pure imaginary ($j^2 = -1$), k represents the wavenumber with ω being angular frequency which is expressed as: $k = \omega/c_0$, and Z_i denotes the acoustic impedance on the i'th surface.

It is generally known that the sound pressure function under the condition of the rigid-wall annular segment cavity can be simply expressed as a product of triple dimensional cosine functions in three directions based on the modal superposition method. It can be written as:

$$p(s,\theta,z) = \sum_{m=0}^{+\infty}\sum_{n=0}^{+\infty}\sum_{l=0}^{+\infty} A^1_{mnl}\cos(\lambda_m s)\cos(\lambda_n\theta)\cos(\lambda_l z) \tag{2}$$

in which $\lambda_m = m\pi/R$, $\lambda_n = n\pi/\phi$, $\lambda_l = l\pi/h$ When the sound pressure expression is used to deal with the impedance boundary conditions, the first derivative of this sound pressure function is not continuous on the surface of cavity. For example, take partial derivative of p with respect to s on the surface of $s = 0$:

$$\left.\frac{\partial p}{\partial s}\right|_{s=0} = \sum_{m=0}^{+\infty}\sum_{n=0}^{+\infty}\sum_{l=0}^{+\infty} A_{mnl}\lambda_m\lambda_n\lambda_l\sin(\lambda_m 0)\cos(\lambda_n\theta)\cos(\lambda_l z) = 0 \tag{3}$$

However, it does not satisfy the boundary value problem of impedance wall which is given in Eq. (1). In order to satisfy various impedance boundary conditions of the annular segment cavity, a 3D-IFSM for the pressure expression is presented to eliminate the discontinuous or jumping phenomenon in the boundaries. The pressure function can be written as follow:

$$p(s,\theta,z,t) = e^{-j\omega t}\left(\mathbf{P}^{\Omega}(s,\theta,z) + \sum_{i=1}^{6}\mathbf{P}_i^{S}(s,\theta,z)\right)\mathbf{H}_p \tag{4}$$

where $\mathbf{P}^{\Omega}$ represents the internal pressure distribution function, and $\mathbf{P}_i^{S}$ expresses the supplementary polynomial of the sound pressure on the i'th surface of the cavity. Their specific expressions are:

$$\mathbf{P}^{\Omega}(s,\theta,z) = \begin{Bmatrix}\cos\lambda_{R0}s\cos\lambda_{\phi 0}\theta\cos\lambda_{h0}z,\ldots,\cos\lambda_{R0}s\cos\lambda_{\phi 0}\theta\cos\lambda_{hL}z,\ldots,\\ \cos\lambda_{R0}s\cos\lambda_{\phi N}\theta\cos\lambda_{hL}z,\ldots,\cos\lambda_{RM}s\cos\lambda_{\phi N}\theta\cos\lambda_{hL}z\end{Bmatrix} \tag{5a}$$

$$\mathbf{P}_1^{S}(s,\theta,z) = \begin{Bmatrix}\xi_1(s)\cos\lambda_{\phi 0}\theta\cos\lambda_{h0}z,\ldots,\xi_1(s)\cos\lambda_{\phi 0}\theta\cos\lambda_{hl}z,\ldots,\\ \xi_1(s)\cos\lambda_{\phi 0}\theta\cos\lambda_{hL}z,\ldots,\xi_1(s)\cos\lambda_{\phi N}\theta\cos\lambda_{hL}z\end{Bmatrix}, \quad \text{on } s=0 \tag{5b}$$

$$\mathbf{P}_2^{S}(s,\theta,z) = \begin{Bmatrix}\xi_2(s)\cos\lambda_{\phi 0}\theta\cos\lambda_{h0}z,\ldots,\xi_2(s)\cos\lambda_{\phi 0}\theta\cos\lambda_{hl}z,\ldots,\\ \xi_2(s)\cos\lambda_{\phi 0}\theta\cos\lambda_{hL}z,\ldots,\xi_2(s)\cos\lambda_{\phi N}\theta\cos\lambda_{hL}z\end{Bmatrix}, \quad \text{on } s=R \tag{5c}$$

$$\mathbf{P}_3^{S}(s,\theta,z) = \begin{Bmatrix}\chi_1(\theta)\cos\lambda_{R0}s\cos\lambda_{h0}z,\ldots,\chi_1(\theta)\cos\lambda_{R0}s\cos\lambda_{hl}z,\ldots,\\ \chi_1(\theta)\cos\lambda_{R0}s\cos\lambda_{hL}z,\ldots,\chi_1(\theta)\cos\lambda_{RM}s\cos\lambda_{hL}z\end{Bmatrix}, \quad \text{on } \theta=0 \tag{5d}$$

$$\mathbf{P}_4^{S}(s,\theta,z) = \begin{Bmatrix}\chi_2(\theta)\cos\lambda_{R0}s\cos\lambda_{h0}z,\ldots,\chi_2(\theta)\cos\lambda_{R0}s\cos\lambda_{hl}z,\ldots,\\ \chi_2(\theta)\cos\lambda_{R0}s\cos\lambda_{hL}z,\ldots,\chi_2(\theta)\cos\lambda_{RM}s\cos\lambda_{hL}z\end{Bmatrix}, \quad \text{on } \theta=\phi \tag{5e}$$

$$\mathbf{P}_5^{S}(s,\theta,z) = \begin{Bmatrix}\zeta_1(z)\cos\lambda_{R0}s\cos\lambda_{\phi 0}\theta,\ldots,\zeta_1(z)\cos\lambda_{R0}s\cos\lambda_{\phi n}\theta,\ldots,\\ \zeta_1(z)\cos\lambda_{R0}s\cos\lambda_{\phi N}\theta,\ldots,\zeta_1(z)\cos\lambda_{RM}s\cos\lambda_{\phi N}\theta\end{Bmatrix}, \quad \text{on } z=0 \tag{5f}$$

$$\mathbf{P}_6^{S}(s,\theta,z) = \begin{Bmatrix}\zeta_2(z)\cos\lambda_{R0}s\cos\lambda_{\phi 0}\theta,\ldots,\zeta_2(z)\cos\lambda_{R0}s\cos\lambda_{\phi n}\theta,\ldots,\\ \zeta_2(z)\cos\lambda_{R0}s\cos\lambda_{\phi N}\theta,\ldots,\zeta_2(z)\cos\lambda_{RM}s\cos\lambda_{\phi N}\theta\end{Bmatrix}, \quad \text{on } z=h \tag{5g}$$

$$\mathbf{H}_p = \begin{Bmatrix}A_{0,0,0},\ldots,A_{0,0,l},\ldots,A_{0,0,L},\ldots,A_{0,N,L},\ldots,A_{m,n,l},\ldots,A_{M,N,L},\\ a^1_{0,0},\ldots,a^1_{0,l},\ldots,a^1_{0,L},\ldots,a^1_{N,L},\ a^2_{0,0},\ldots,a^2_{0,l},\ldots,a^2_{0,L},\ldots,a^2_{N,L},\\ b^1_{0,0},\ldots,b^1_{0,l},\ldots,b^1_{0,L},\ldots,b^1_{M,L},\ b^2_{0,0},\ldots,b^2_{0,l},\ldots,b^2_{0,L},\ldots,b^2_{M,L},\\ c^1_{0,0},\ldots,c^1_{0,n},\ldots,c^1_{0,N},\ldots,c^1_{M,N},\ c^2_{0,0},\ldots,c^2_{0,n},\ldots,c^2_{0,N},\ldots,c^2_{M,N}\end{Bmatrix}^T \tag{6}$$

in which $\lambda_{Rm} = m\pi/R$, $\lambda_{\phi n} = n\pi/\phi$, $\lambda_{hl} = l\pi/h$ The 3D Fourier coefficient can be expressed as A_{mnl}. The 2D unknown coefficients of six auxiliary functions are a^1_{nl}, a^2_{nl}, b^1_{ml}, b^2_{ml}, c^1_{mn} and c^2_{mn}. Six auxiliary functions $\xi_1(s)$, $\xi_2(s)$, $\chi_1(\theta)$, $\chi_2(\theta)$, $\zeta_1(z)$ and $\zeta_2(z)$ are introduced to eliminate the differential discontinuity of sound pressure function at each impedance wall. They can be given as:

$$\xi_1(s) = \frac{R}{2\pi}\sin\left(\frac{\pi s}{2R}\right) + \frac{R}{2\pi}\sin\left(\frac{3\pi s}{2R}\right) \tag{7a}$$

$$\xi_2(s) = -\frac{R}{2\pi}\cos\left(\frac{\pi s}{2R}\right) + \frac{R}{2\pi}\cos\left(\frac{3\pi s}{2R}\right) \tag{7b}$$

$$\chi_1(\theta) = \frac{\phi}{2\pi}\sin\left(\frac{\pi\theta}{2\phi}\right) + \frac{\phi}{2\pi}\sin\left(\frac{3\pi\theta}{2\phi}\right) \tag{7c}$$

$$\chi_2(\theta) = -\frac{\phi}{2\pi}\cos\left(\frac{\pi\theta}{2\phi}\right) + \frac{\phi}{2\pi}\cos\left(\frac{3\pi\theta}{2\phi}\right) \tag{7d}$$

$$\zeta_1(z) = \frac{h}{2\pi}\sin\left(\frac{\pi z}{2h}\right) + \frac{h}{2\pi}\sin\left(\frac{3\pi z}{2h}\right) \tag{7e}$$

$$\zeta_2(z) = -\frac{h}{2\pi}\cos\left(\frac{\pi z}{2h}\right) + \frac{h}{2\pi}\cos\left(\frac{3\pi z}{2h}\right) \tag{7f}$$

It is easy to verify that

$$\xi_1(0) = \xi_1(R) = \xi_1'(R) = 0, \quad \xi_1'(0) = 1 \tag{8a}$$

$$\xi_2(0) = \xi_2(R) = \xi_2'(0) = 0, \quad \xi_2'(R) = 1 \tag{8b}$$

$$\chi_1(0) = \chi_1(\phi) = \chi_1'(\phi) = 0, \quad \chi_1'(0) = 1 \tag{8c}$$

$$\chi_2(0) = \chi_2(\phi) = \chi_2'(0) = 0, \quad \chi_2'(\phi) = 1 \tag{8d}$$

$$\zeta_1(0) = \zeta_1(h) = \zeta_1'(h) = 0, \quad \zeta_1'(0) = 1 \tag{8e}$$

$$\zeta_2(0) = \zeta_2(h) = \zeta_2'(0) = 0, \quad \zeta_2'(h) = 1 \tag{8f}$$

We can easily find that the addition of polynomial can satisfy the impedance boundary value problem. For example, take partial

derivative of p with respect to s on the surface of $s = 0$:

$$\left.\frac{\partial p}{\partial s}\right|_{s=0} = \sum\sum a_{nl}^{1}\cos\lambda_{\phi n}\theta\cos\lambda_{hl}z \tag{9}$$

This kind of 3D-FSM sound pressure distribution function can ensure the first derivative of sound pressure is continuous at any point of the whole solution domain. It is different from the product of three one-dimensional modified forms [42,43], which can be further extended to deal with the non-uniform impedance wall.

Energy expressions

The main work of this paper is to investigate the acoustic modes and responses of the annular segment cavity with various impedance boundary conditions. Thus, we study the 3D sound field characteristics of the cavity on the basis of Rayleigh–Ritz energy method to obtain more accurate results. This energy technology is more preferred to obtain than the technology based on solving the Helmholtz equation and general boundary conditions directly as long as it is constructed sufficiently smooth over the entire solution domain.

The Lagrangian function (L) for the acoustic cavity with the various impedance boundary constraints can be written as:

$$L = U - T - W_{wall} - W_S \tag{10}$$

where U represents the total acoustic potential energy, T denotes the total kinetic energy, W_{wall} expresses the dissipated acoustic energy on impedance surfaces, and W_S shows the work done by the sound source which is placed in the internal cavity. In the following part, we will give the concrete expressions all of them [44,45].

The total acoustic potential energy (U) which is stored in the annular segment cavity can be given as:

$$\begin{aligned} U &= \frac{1}{2\rho c_0^2}\int_V p^2(s,\theta,z)dV \\ &= \frac{1}{2\rho c_0^2}\int_0^R\int_0^\phi\int_0^h\left\{\left(\mathbf{P}^{\Omega}(s,\theta,z)+\sum_{i=1}^{6}\mathbf{P}_i^{S}(s,\theta,z)\right)\mathbf{H}_p\right\}^2(s+R_2)dsd\theta dz \end{aligned} \tag{11}$$

where ρ is the mass density of the acoustic in the annular segment cavity, c_0 is the speed of sound propagation in the medium, p expresses the acoustic pressure, and V represents the volume of the cavity.

The total kinetic energy (T) of the annular segment cavity can be written as:

$$\begin{aligned} T &= \frac{1}{2\rho\omega^2}\int_V (gradp)^2dV \\ &= \frac{1}{2\rho\omega^2}\int_0^R\int_0^\phi\int_0^h\left\{\begin{array}{l}\left[\left(\frac{\partial\mathbf{P}^{\Omega}(s,\theta,z)}{\partial s}+\sum_{i=1}^{6}\frac{\partial\mathbf{P}_i^{S}(s,\theta,z)}{\partial s}\right)\mathbf{H}_p\right]^2 \\ +\left[\left(\frac{\partial\mathbf{P}^{\Omega}(s,\theta,z)}{(s+R_2)\partial\theta}+\sum_{i=1}^{6}\frac{\partial\mathbf{P}_i^{S}(s,\theta,z)}{(s+R_2)\partial\theta}\right)\mathbf{H}_p\right]^2 \\ \left[\left(\frac{\partial\mathbf{P}^{\Omega}(s,\theta,z)}{\partial z}+\sum_{i=1}^{6}\frac{\partial\mathbf{P}_i^{S}(s,\theta,z)}{\partial z}\right)\mathbf{H}_p\right]^2\end{array}\right\} \\ &\quad (s+R_2)dsd\theta dz \end{aligned} \tag{12}$$

in which ω represents the angular frequency of the cavity, R_2 is the inner radius of this considered cavity model, and **grad**p expresses the sound pressure gradient.

According to the boundary value problem which is shown in the Eq. (1), the dissipated acoustic energy of the impedance wall (W_{wall}) can be expressed as:

$$\begin{aligned} W_{wall} &= -\frac{1}{2}\sum_{i=1}^{6}\int_{S_i}\frac{p^2}{j\omega Z_i}dS_i \\ &= -\frac{1}{2}\left\{\begin{array}{l}\int_{S_1}\frac{[(\mathbf{P}^{\Omega}(s,\theta,z)+\sum_{i=1}^{6}\mathbf{P}_i^{S}(s,\theta,z))\mathbf{H}_p]^2}{j\omega Z_1}dS_1|_{s=0} \\ +\int_{S_2}\frac{[(\mathbf{P}^{\Omega}(s,\theta,z)+\sum_{i=1}^{6}\mathbf{P}_i^{S}(s,\theta,z))\mathbf{H}_p]^2}{j\omega Z_2}dS_2|_{s=R} \\ +\int_{S_3}\frac{[(\mathbf{P}^{\Omega}(s,\theta,z)+\sum_{i=1}^{6}\mathbf{P}_i^{S}(s,\theta,z))\mathbf{H}_p]^2}{j\omega Z_3}dS_3|_{\theta=0} \\ +\int_{S_4}\frac{[(\mathbf{P}^{\Omega}(s,\theta,z)+\sum_{i=1}^{6}\mathbf{P}_i^{S}(s,\theta,z))\mathbf{H}_p]^2}{j\omega Z_4}dS_4|_{\theta=\phi} \\ +\int_{S_5}\frac{[(\mathbf{P}^{\Omega}(s,\theta,z)+\sum_{i=1}^{6}\mathbf{P}_i^{S}(s,\theta,z))\mathbf{H}_p]^2}{j\omega Z_5}dS_5|_{z=0} \\ +\int_{S_6}\frac{[(\mathbf{P}^{\Omega}(s,\theta,z)+\sum_{i=1}^{6}\mathbf{P}_i^{S}(s,\theta,z))\mathbf{H}_p]^2}{j\omega Z_6}dS_6|_{z=h}\end{array}\right\} \end{aligned} \tag{13}$$

in which j is the pure imaginary ($j^2 = -1$), i is the number of the impedance wall, and Z_i (i = 1, 2, 3, 4, 5, 6) shows the complex acoustic impedance which is set on the i'th wall surface. Besides, S_i (i = 1, 2, 3, 4, 5, 6) donates the area of i'th wall surface.

The work done by the monopole source (W_S) is given as:

$$W_S = -\int_0^R\int_0^\phi\int_0^h\frac{(\mathbf{P}^{\Omega}(s,\theta,z)+\sum_{i=1}^{6}\mathbf{P}_i^{S}(s,\theta,z))\mathbf{H}_pQ}{j\omega}(s+R_2)dsd\theta dz \tag{14}$$

where Q expresses the distribution function of the source intensity.

As an acoustic point source corresponds to a pulsating sphere, the incident pressure can be written as:

$$p^0 = A\frac{e^{-jkR_0}}{R_0} \tag{15}$$

where A is the amplitude of the source (in kg/s^2), R_0 is the distance from the source and k is the wave number. Alternatively, the monopole can also be characterized by its volume velocity Q_0 (in m^3/s). The relation between the source amplitude A and volume velocity Q_0 is:

$$Q_0 = \frac{4\pi A}{j\rho c_0 k} \tag{16}$$

where ρc_0 is characteristic impedance of the cavity. As a point sound source which is located at (s θ z) inside the annular enclosure, Q can be written as:

$$Q = \frac{4\pi A}{j\rho c_0 k}\delta(s-s_0)\delta(\theta-\theta_0)\delta(z-z_0) \tag{17}$$

in which δ is 3-D Dirac function.

Partial derivation of Lagrange equation (L) against the unknown 3D Fourier coefficient is zero, which can be expressed as follows:

$$\frac{\partial U}{\partial\mathbf{H}_p}-\frac{\partial T}{\partial\mathbf{H}_p}-\frac{\partial W_{wall}}{\partial\mathbf{H}_p} = \frac{\partial W_S}{\partial\mathbf{H}_p} \tag{18}$$

Substitute Eqs. (4)–(8), (11)–(17) into Eq. (18) and a matrix form can be obtained based on the Rayleigh-Ritz technology.

$$(\mathbf{K}+\omega\mathbf{Z}+\omega^2\mathbf{M})\mathbf{H}_p = \mathbf{F} \tag{19}$$

where **K**, **M**, **Z** and **F** are the stiffness matrix, mass matrix, impedance matrix and force vector which can be written separately as follows:

$$\mathbf{K} = \begin{bmatrix} \mathbf{K}_{1-1} & \mathbf{K}_{1-2} & \mathbf{K}_{1-3} & \mathbf{K}_{1-4} & \mathbf{K}_{1-5} & \mathbf{K}_{1-6} & \mathbf{K}_{1-7} \\ \mathbf{K}_{1-2}^T & \mathbf{K}_{2-2} & \mathbf{K}_{2-3} & \mathbf{K}_{2-4} & \mathbf{K}_{2-5} & \mathbf{K}_{2-6} & \mathbf{K}_{2-7} \\ \mathbf{K}_{1-3}^T & \mathbf{K}_{2-3}^T & \mathbf{K}_{3-3} & \mathbf{K}_{3-4} & \mathbf{K}_{3-5} & \mathbf{K}_{3-6} & \mathbf{K}_{3-7} \\ \mathbf{K}_{1-4}^T & \mathbf{K}_{2-4}^T & \mathbf{K}_{3-4}^T & \mathbf{K}_{4-4} & \mathbf{K}_{4-5} & \mathbf{K}_{4-6} & \mathbf{K}_{4-7} \\ \mathbf{K}_{1-5}^T & \mathbf{K}_{2-5}^T & \mathbf{K}_{3-5}^T & \mathbf{K}_{4-5}^T & \mathbf{K}_{5-5} & \mathbf{K}_{5-6} & \mathbf{K}_{5-7} \\ \mathbf{K}_{1-6}^T & \mathbf{K}_{2-6}^T & \mathbf{K}_{3-6}^T & \mathbf{K}_{4-6}^T & \mathbf{K}_{5-6}^T & \mathbf{K}_{6-6} & \mathbf{K}_{6-7} \\ \mathbf{K}_{1-7}^T & \mathbf{K}_{2-7}^T & \mathbf{K}_{3-7}^T & \mathbf{K}_{4-7}^T & \mathbf{K}_{5-7}^T & \mathbf{K}_{6-7}^T & \mathbf{K}_{7-7} \end{bmatrix} \tag{20}$$

Table 1
Convergence and accuracy of natural frequencies f for annular segment cavity with the rigid wall.

$M \times N \times L$	Mode number							
	1	2	3	4	5	6	7	8
3 × 3 × 3	0.000	85.000	145.089	168.153	170.000	223.497	255.000	280.046
4 × 4 × 4	0.000	85.000	145.088	168.152	170.000	223.497	255.000	280.045
5 × 5 × 5	0.000	85.000	145.088	168.152	170.000	223.497	255.000	280.045
6 × 6 × 6	0.000	85.000	145.088	168.152	170.000	223.497	255.000	280.045
7 × 7 × 7	0.000	85.000	145.088	168.152	170.000	223.497	255.000	280.045
8 × 8 × 8	0.000	85.000	145.088	168.152	170.000	223.497	255.000	280.045
Exact [47]	0.000	85.000	145.087	168.152	170.000	223.495	255.000	280.044
FEM	0.000	85.022	145.138	168.207	170.175	223.661	255.590	280.318

$$\mathbf{Z} = \begin{bmatrix} \mathbf{Z}_{1-1} & \mathbf{Z}_{1-2} & \mathbf{Z}_{1-3} & \mathbf{Z}_{1-4} & \mathbf{Z}_{1-5} & \mathbf{Z}_{1-6} & \mathbf{Z}_{1-7} \\ \mathbf{Z}_{1-2}^T & \mathbf{Z}_{2-2} & \mathbf{Z}_{2-3} & \mathbf{Z}_{2-4} & \mathbf{Z}_{2-5} & \mathbf{Z}_{2-6} & \mathbf{Z}_{2-7} \\ \mathbf{Z}_{1-3}^T & \mathbf{Z}_{2-3}^T & \mathbf{Z}_{3-3} & \mathbf{Z}_{3-4} & \mathbf{Z}_{3-5} & \mathbf{Z}_{3-6} & \mathbf{Z}_{3-7} \\ \mathbf{Z}_{1-4}^T & \mathbf{Z}_{2-4}^T & \mathbf{Z}_{3-4}^T & \mathbf{Z}_{4-4} & \mathbf{Z}_{4-5} & \mathbf{Z}_{4-6} & \mathbf{Z}_{4-7} \\ \mathbf{Z}_{1-5}^T & \mathbf{Z}_{2-5}^T & \mathbf{Z}_{3-5}^T & \mathbf{Z}_{4-5}^T & \mathbf{Z}_{5-5} & \mathbf{Z}_{5-6} & \mathbf{Z}_{5-7} \\ \mathbf{Z}_{1-6}^T & \mathbf{Z}_{2-6}^T & \mathbf{Z}_{3-6}^T & \mathbf{Z}_{4-6}^T & \mathbf{Z}_{5-6}^T & \mathbf{Z}_{6-6} & \mathbf{Z}_{6-7} \\ \mathbf{Z}_{1-7}^T & \mathbf{Z}_{2-7}^T & \mathbf{Z}_{3-7}^T & \mathbf{Z}_{4-7}^T & \mathbf{Z}_{5-7}^T & \mathbf{Z}_{6-7}^T & \mathbf{Z}_{7-7} \end{bmatrix} \tag{21}$$

$$\mathbf{M} = \begin{bmatrix} \mathbf{M}_{1-1} & \mathbf{M}_{1-2} & \mathbf{M}_{1-3} & \mathbf{M}_{1-4} & \mathbf{M}_{1-5} & \mathbf{M}_{1-6} & \mathbf{M}_{1-7} \\ \mathbf{M}_{1-2}^T & \mathbf{M}_{2-2} & \mathbf{M}_{2-3} & \mathbf{M}_{2-4} & \mathbf{M}_{2-5} & \mathbf{M}_{2-6} & \mathbf{M}_{2-7} \\ \mathbf{M}_{1-3}^T & \mathbf{M}_{2-3}^T & \mathbf{M}_{3-3} & \mathbf{M}_{3-4} & \mathbf{M}_{3-5} & \mathbf{M}_{3-6} & \mathbf{M}_{3-7} \\ \mathbf{M}_{1-4}^T & \mathbf{M}_{2-4}^T & \mathbf{M}_{3-4}^T & \mathbf{M}_{4-4} & \mathbf{M}_{4-5} & \mathbf{M}_{4-6} & \mathbf{M}_{4-7} \\ \mathbf{M}_{1-5}^T & \mathbf{M}_{2-5}^T & \mathbf{M}_{3-5}^T & \mathbf{M}_{4-5}^T & \mathbf{M}_{5-5} & \mathbf{M}_{5-6} & \mathbf{M}_{5-7} \\ \mathbf{M}_{1-6}^T & \mathbf{M}_{2-6}^T & \mathbf{M}_{3-6}^T & \mathbf{M}_{4-6}^T & \mathbf{M}_{5-6}^T & \mathbf{M}_{6-6} & \mathbf{M}_{6-7} \\ \mathbf{M}_{1-7}^T & \mathbf{M}_{2-7}^T & \mathbf{M}_{3-7}^T & \mathbf{M}_{4-7}^T & \mathbf{M}_{5-7}^T & \mathbf{M}_{6-7}^T & \mathbf{M}_{7-7} \end{bmatrix} \tag{22}$$

$$\mathbf{F} = [\mathbf{F}_1 \quad \mathbf{F}_2 \quad \mathbf{F}_3 \quad \mathbf{F}_4 \quad \mathbf{F}_5 \quad \mathbf{F}_6 \quad \mathbf{F}_7]^T \tag{23}$$

The detailed expressions for these matrices are given in Appendix. When the modal characteristics of closed space are studied, we only need to set the right side of the Eq. (19) to zero. However, it is a nonlinear eigenvalue problem because the equation contains both the first and quadratic term of the angular frequency. So we should do the further transform, $\mathbf{Y} = \omega \mathbf{H}_p$, to get a linear equation which can be expressed as follows [16,46]:

$$(\mathbf{R} - \omega \mathbf{S})\mathbf{G} = \mathbf{0} \tag{24}$$

where:

$$\mathbf{R} = \begin{bmatrix} \mathbf{0} & -\mathbf{K} \\ -\mathbf{K} & -\mathbf{Z} \end{bmatrix}; \quad \mathbf{S} = \begin{bmatrix} -\mathbf{K} & \mathbf{0} \\ \mathbf{0} & \mathbf{M} \end{bmatrix}; \quad \mathbf{G} = \begin{pmatrix} \mathbf{H}_p \\ \mathbf{Y} \end{pmatrix} \tag{25}$$

By solving the Eq. (24), we can easily obtain the natural frequencies and coefficients ($\mathbf{H}_p$) which are the eigenvalues and eigenvectors of the standard matrix. Then we can obtain the corresponding mode shapes from Eq. (24). Besides, substituting $\mathbf{H}_p$ into the Eq. (4), the sound pressure for the annular segment cavity model can be immediately obtained.

Numerical results and discussion

In the first section of the numerical analysis, the modal characteristics of the annular segment cavity are given which contain natural frequencies and mode shapes. In the second section, the present method is used to predict the acoustic response under the excitation of a monopole sound source.

Convergence study and modal analysis

This section mainly discusses the natural characteristics of the cavity with rigid walls. In the numerical calculation process, the simulation of rigid wall will be realized when the wall impedance is assumed to be an infinite pure imaginary ($10^{10}j$). It is the first time to study the annular segment cavity using the present method, so it is necessary to study its convergence and accuracy firstly. As previously mentioned in the Eq. (4), the series expansions of the sound pressure function can be obtained by truncating numbers of term M and N in numerical calculations. The size of the values of M and N is the direct representation of the convergence of the present method. The accuracy of present method is verified by comparing with the results obtained by FEM and analytic method. The natural frequency expression of analytic solutions for annular segment cavity with rigid wall is given as [47]:

$$f_{iqk} = \frac{c_0}{2\pi}\left(\frac{\lambda_{qk}}{R_1^2} + \frac{i^2\pi^2}{L^2}\right)^{1/2} \tag{26}$$

where index i is (0, 1, 2…), and index k is (0, 1, 2…). The index q can be chosen as:

$$q = \frac{180°n}{\varphi}; \quad \begin{cases} 0 < \varphi \leqslant 360° \\ n = 0, 1, 2, \ldots \end{cases} \tag{27}$$

in which φ is measured in degree. It should be pointed out that q will be integer only if φ is a submultiple of 180°n. For non-integer q, λ_{qk} is obtained by interpolation which can refer to the Reference [47]. When $R_2/R_1 > 0.5$, the index λ_{qk} can be written as:

$$\lambda_{qk} \approx \left(\frac{k\pi R_1}{R_1 - R_2}\right)^2 + \left(\frac{2jR_1}{R_1 + R_2}\right)^2 \tag{28}$$

Table 1 shows the convergence of first eight natural frequencies f of the annular segment cavity with the rigid wall. The geometrical dimensions are $R_2/R_1 = 0.5$, $\phi = 90°$, and $h = 2$, separately. The mass density and the speed of sound propagation in the air cavity are $\rho = 1.21\ \mathrm{kg/m^3}$ and $c_0 = 340\ \mathrm{m/s}$. As shown in Table 1, the present method shows the fast convergence. The biggest difference for the worst case which is made the contrast of 3 × 3 × 3 and 8 × 8 × 8 is less than 0.0007%. Then the biggest difference for the worst case which is made the contrast of 4 × 4 × 4 and 8 × 8 × 8 is zero. In addition, the exact solutions and simulation results of the FEM are also given here to make contrast. It can be seen that the solution obtained by the present method is closer to the exact solution than that obtained by FEM because the FEM has a high requirement of the mesh quality and the solver is an approximate numerical algorithm.

It is generally known that the changes of the geometric parameters will directly affect the natural characteristics of the cavity. It is of great significance for vibration and noise reduction to study the effects of geometric parameters on the natural frequencies of annular segment cavities. As shown in Table 2, the natural frequencies f from the second to the ninth order of annular segment cavities on the rigid walls are given. The cavities have various sector angles ϕ and radius ratios R_2/R_1. Since the first order natural frequency value is zero, it is not considered in this table. The geometrical dimensions are $R_2/R_1 = 0.6$ and 0.3, $\phi = 90°$, 240° and 360°, and $h = 2$, separately. The mass density and the speed of sound propagation in the medium of the acoustic are the same

Table 2
The natural frequencies f for annular segment cavity with various sector angle ϕ and radius ratio R_2/R_1.

R_2/R_1	ϕ	Method	Mode number							
			2	3	4	5	6	7	8	9
0.6	90°	Present	85.000	136.146	160.498	170.000	217.795	255.000	268.925	282.036
		Exact [47]	85.000	135.282	159.769	170.000	217.258	255.000	270.563	283.601
		Error (%)	0.000	0.635	0.454	0.000	0.247	0.000	0.609	0.555
		FEM	85.039	136.233	160.596	170.311	218.094	256.050	269.424	282.526
		Error (%)	0.046	0.064	0.061	0.183	0.137	0.412	0.186	0.174
	240°	Present	51.243	85.000	99.252	102.300	133.005	152.987	170.000	175.013
		Exact [47]	50.731	85.000	98.988	101.461	132.361	152.192	170.000	174.320
		Error (%)	0.999	0.000	0.266	0.820	0.484	0.520	0.000	0.396
		FEM	51.350	85.039	99.340	102.639	133.291	153.809	170.311	175.752
		Error (%)	0.209	0.046	0.089	0.331	0.215	0.537	0.183	0.422
	360°	Present	68.295	85.000	109.035	136.146	160.501	170.000	183.203	203.134
		Exact [47]	67.641	85.000	108.629	135.282	159.769	170.000	182.963	202.923
		Error (%)	0.958	0.000	0.372	0.635	0.456	0.000	0.131	0.104
		FEM	68.371	85.039	109.082	136.233	160.596	170.311	183.502	203.372
		Error (%)	0.112	0.046	0.041	0.065	0.060	0.183	0.162	0.116
0.3	90°	Present	85.000	160.636	170.000	181.738	233.889	254.641	255.000	268.453
		FEM	85.010	160.684	170.078	181.786	233.978	254.755	255.262	268.564
		Error (%)	0.012	0.030	0.046	0.026	0.038	0.045	0.103	0.041
	240°	Present	64.963	85.000	106.985	124.634	150.856	170.000	177.683	181.992
		FEM	65.035	85.022	107.043	124.823	151.028	170.175	178.093	182.179
		Error (%)	0.111	0.026	0.054	0.152	0.114	0.103	0.231	0.103
	360°	Present	85.000	85.613	120.642	160.633	170.000	181.736	190.341	226.199
		Exact [47]	85.000	85.612	120.641	160.634	170.000	181.736	190.340	226.196
		Error (%)	0.000	0.001	0.001	0.001	0.000	0.000	0.001	0.001
		FEM	85.039	85.637	120.687	160.723	170.311	181.834	190.629	226.412
		Error (%)	0.046	0.028	0.037	0.056	0.183	0.054	0.151	0.094

as Table 1. As we can see from Table 2, the natural frequencies of the present method show good agreement with other two methods. Besides, the natural frequencies of the studied model are affected a lot by the change of various sector angles ϕ and radius ratios R_2/R_1. We also find that the natural frequencies of the annular segment cavity increase with the decrease of the radius ratios R_2/R_1. The number of frequencies increases significantly within the fixed interval when ϕ increases. Thus, it is conducive to vibration reduction when the annular segment cavity with smaller radius ratio and smaller sector angle is adopted.

For a closed cavity, it can effectively avoid the resonance frequency when the medium inside of cavity changes. Table 3 gives the second to the eight order of natural frequencies f of the cavity with different mediums and various cavity depths h. Two types of mediums, air and water, are considered. The mass density and the speed of sound propagation in the air cavity are the same as Table 1. The mass density and the speed of sound propagation in the water cavity are $\rho_{water} = 1000\,\mathrm{kg/m^3}$ and $c_{water} = 1480\,\mathrm{m/s}$. In addition, five kinds of cavity depths h are considered, including 2 m, 1.5 m, 1 m, 0.5 m and 0.1 m. The other geometrical dimensions are: $R_2/R_1 = 0.5$ and $\phi = 90°$. Some results are found in this table. First, the results obtained by this

Table 3
The natural frequencies f for annular segment cavity with various cavity depths h and medium.

Medium	h	Method	Mode number						
			2	3	4	5	6	7	8
Air	2	Present	85.000	145.088	168.152	170.000	223.497	255.000	280.045
		FEM	84.998	145.122	168.236	169.977	223.677	254.904	279.875
	1.5	Present	113.333	145.087	184.105	226.667	269.125	280.046	302.110
		FEM	113.327	145.121	184.224	226.594	269.369	279.883	302.244
	1	Present	145.087	170.000	223.496	280.046	327.606	340.000	345.951
		FEM	145.115	169.979	223.642	279.856	327.991	339.695	344.799
	0.5	Present	145.087	280.046	340.000	345.951	369.662	382.175	403.798
		FEM	145.109	279.915	339.547	345.178	369.723	382.023	403.666
	0.1	Present	145.087	280.046	345.951	382.175	403.798	478.165	521.550
		FEM	145.090	280.049	345.957	382.182	403.804	478.209	521.567
Water	2	Present	370.000	631.557	731.959	740.000	972.864	1110.000	1219.024
		FEM	369.991	631.708	732.320	739.899	973.654	1109.582	1218.280
	1.5	Present	493.333	631.557	801.400	986.667	1171.484	1219.024	1315.066
		FEM	493.306	631.703	801.906	986.350	1172.549	1218.313	1315.649
	1	Present	631.557	740.000	972.864	1219.024	1426.050	1480.000	1505.905
		FEM	631.678	739.908	973.502	1218.198	1427.724	1478.672	1500.888
	0.5	Present	631.557	1219.024	1480.000	1505.905	1609.119	1663.586	1757.709
		FEM	631.653	1218.454	1478.027	1502.539	1609.384	1662.923	1757.135
	0.1	Present	631.557	1219.024	1505.905	1663.586	1757.709	2081.426	2270.278
		FEM	631.569	1219.035	1505.930	1663.616	1757.736	2081.616	2270.351

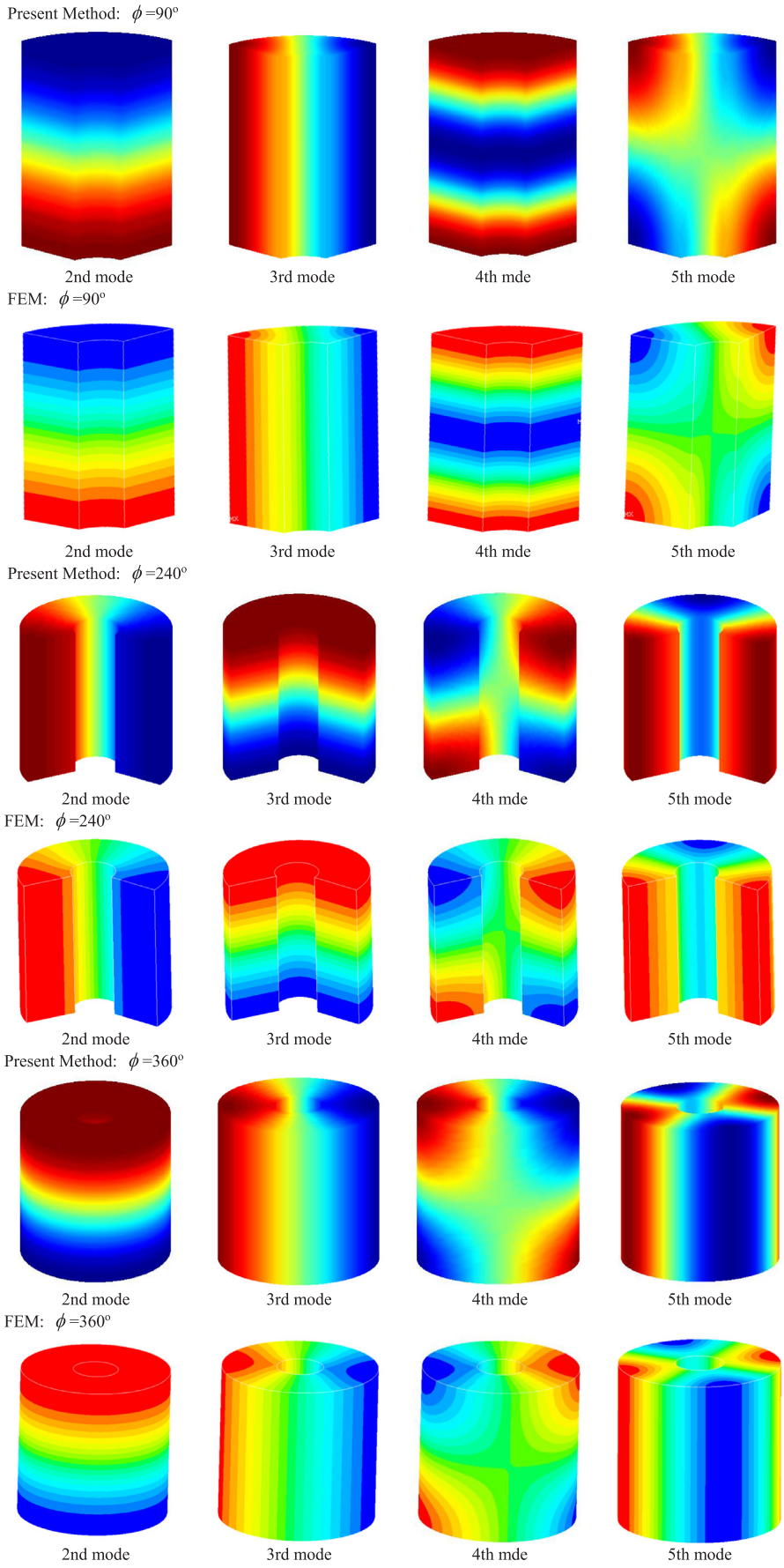

Fig. 2. The mode shapes of the rigid annular segment cavity with different sector angle ϕ.

method are in good agreement with the results obtained by FEM. Second, the medium has a great effect on the natural frequency of cavity. The specific performance is that the frequency of the water cavity is generally higher than the frequency of the air cavity. Third, the values of the frequency increase with the decrease of the cavity depths h. It indicates that the low-frequency resonance can be effectively avoided in the acoustic design by reducing the cavity depth or changing media properties appropriately.

According to the above results, some of the 3D view mode shapes of the rigid annular segment cavity are given in Fig. 2. Sometimes they can more intuitively represent the natural characteristics of cavities. The geometric dimensions of the cavity in these figures are $R_2/R_1 = 0.3$, $\phi = 90°$, 240° and 360°, and $h = 2$, separately. The air properties are consistent with the above studied model. These 3D views of mode shapes are conducive to enhancing our understanding of the acoustic characteristics of the annular segment cavity with rigid walls.

The acoustic response study

Acoustic pressure response is an expression form of acoustic characteristics. The study on acoustic response of the annular segment cavity is a fundamental problem and an important content in acoustic research. In this section, the acoustic response of the annular segment cavity is predicted under the excitation of a monopole sound source. First of all, the physical parameters of the air cavity are same in the following cases. Specifically, the mass density and the speed of sound propagation in the air cavity are $\rho_{air} = 1.21\ \mathrm{kg/m^3}$ and $c_{air} = 340\ \mathrm{m/s}$. And the mass density and the speed of sound propagation in the water cavity are $\rho_{water} = 1000\ \mathrm{kg/m^3}$ and $c_{water} = 1480\ \mathrm{m/s}$. A monopole source is located at one corner of the annular segment cavity. In the following case analysis, the unit sound amplitude of the point source is given directly ($A = 1\ \mathrm{kg/s^2}$) and no special explanation will be given.

In order to overcome the numerical instability caused by the acoustic resonance of the modal frequency, the modal damping coefficient in this paper is employed which can be represented as ξ. As presented by Johnson et al. [48], the damping coefficient can be introduced by using complex wavenumber for the smaller acoustic modal damping ratio which can be expressed as $\widetilde{k} = k(1-j\xi)$. In this paper, damp can be applied by the complex sound velocity whose expression is $\widetilde{c} = c_0(1-j\eta)$. By using the equivalence relation between complex wavenumber and complex sound velocity, we can get a formula:

$$\eta = -\frac{\xi}{1-j\xi} \tag{29}$$

There is no dissipation of sound pressure at the rigid wall which is an ideal acoustic boundary condition. So it is necessary to study the acoustic response of the annular segment cavity with the rigid wall. In Fig. 3, a monopole source is located at one corner of the annular segment air cavity (0.165, 64.54°, 0.2). The positions of the two observation points are at (0.435, 67.62°, 1) and (0.157, 23.2°, 1.5) which are inside the cavity with rigid walls. The geometrical dimensions of the annular segment cavity are $R_2/R_1 = 0.3$, $\phi = 90°$, and $h = 2$, separately. The modal damping coefficient ξ is 0.001. Two results of the cavity in the frequency range of 0–350 Hz are given in Fig. 3, which come from the FEM and the present method. These results show that the present method can predict the same sound pressure responses as FEM with the direct introduction of the acoustic modal damping coefficient whether in the resonance or non-resonance. It shows that the modeling method proposed in this paper can accurately forecast the pressure response of rigid walls, and it is entirely feasible to replace damp by introducing the complex velocity. Although the sound pressure responses at different observation points are different, there are certain attenuations at the resonance peaks with the increase of frequencies. This may be caused by the influence of the medium inside the cavity. In order to compare the effect of medium of cavity on the sound pressure response, Fig. 4 shows the sound pressure response of the water cavity in the frequency range of 0–1500 Hz. The cavity model and observation points are unchanged. The results obtained by the present method are compared with the results of FEM, which shows good agreement. It is not difficult to find that the natural frequencies of the water cavity are much larger than those of the air cavity. When the value of the abscissa is ignored, the shapes of the response curves of the water cavity and the air cavity are identical at the same observation position. What's more, the attenuation of wave crest is more obvious for the water cavity than the air cavity. And then the effect of medium on attenuation of acoustic pressure is proved.

As a dissipative wall, the impedance wall can absorb a part of the sound pressure. It is conducive to the design of acoustic noise reduction. First of all, it is necessary to verify the accuracy of the annular segment cavity model with the impedance wall established in this paper. Fig. 5 focuses on the effect of the impedance-wall on the acoustic pressure responses at different observation points. The location of the sound source is ($R/10$, $\phi/10$, $h/10$). The geometrical dimensions of the air

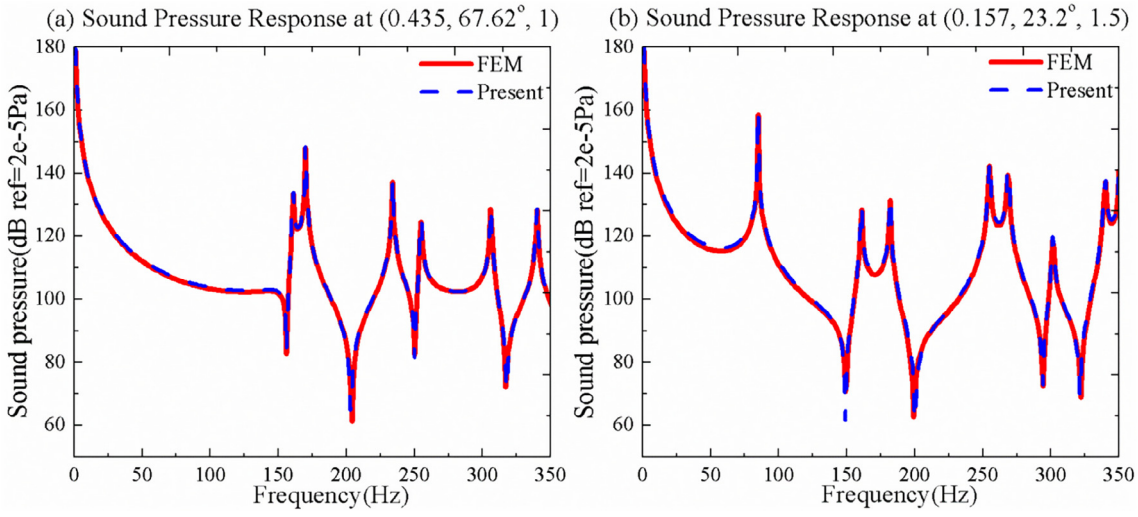

Fig. 3. Sound pressure responses inside the rigid annular segment air cavity at: (a) (0.435, 67.62°, 1) and (b) (0.157, 23.2°, 1.5).

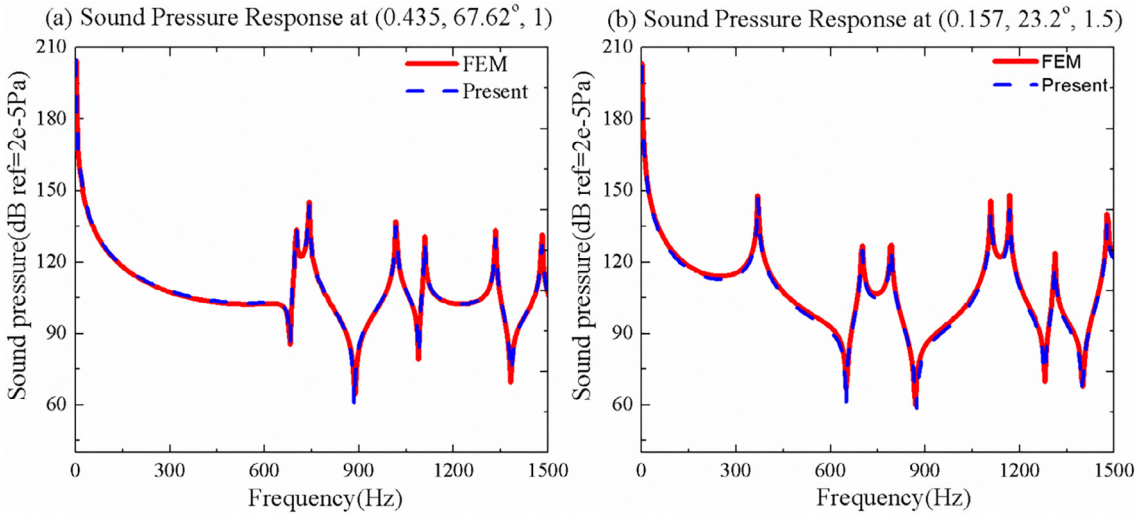

Fig. 4. Sound pressure responses inside the rigid annular segment water cavity at: (a) (0.435, 67.62°, 1) and (b) (0.157, 23.2°, 1.5).

cavity are the same as those in Fig. 3. In this studied model, the complex impedance value $Z = \rho c_0(100\text{-}j)$ is specified on the wall of $z = h$, and other five walls remain rigid boundary conditions. In this case, four results in the frequency range of 0–300 Hz are given based on the two observation points at (0.35, 45.48°, 1) and (0.47, 45.19°, 1.9) inside the cavity. To check the correctness of this method, the simulation results of the FEM are also given as a comparison and the results show good agreement of them. We can see from these curves that the sound pressure level decreases continuously with the increase of frequency. Besides, it is not difficult to find that the sound pressure response continues to decay.

In order to understand the effect of the impedance value on the pressure response, the sound pressure response with the different impedance boundary constraints at the same observation point is given in Fig. 6. To make the contrast even more remarkable, the sound pressure response curves with the six rigid walls are also given in the figures. The geometrical dimensions of the annular segment cavity are $R_2/R_1 = 0.5$, $\phi = 90°$, and $h = 2$, separately. The point source is placed at ($R/10$, $\phi/10$, $h/10$). The positions of the two observation points are at ($3R/10$, $4\phi/10$, $5h/10$) and ($8R/10$, $8\phi/10$, $8h/10$). The modal damping coefficient ξ is 0.001. The two values of impedance walls are $Z_1 = \rho c_0(100\text{-}j)$ and $Z_2 = \rho c_0(10\text{-}j)$ on $z = 0$ and $z = h$. The other four walls still remain rigid boundary conditions. Three results of the air cavity in the frequency range of 0–300 Hz are given to make comparison in (a) and (b) of Fig. 6. And the sound pressure responses of the water cavity in the frequency range of 0–1500 Hz are given in (c) and (d) of Fig. 6. The results show that the addition of impedance wall can effectively reduce the peak value of resonance region. Besides, there is an interesting finding in these figures that he change of these two kinds of impedance values only affects the peak value of the pressure response curve at the same observation point, and the curve is smoother while the real part of the impedance decreases. It shows that the pursuit of a new material with less impedance value is of great significance for shock absorption and noise reduction.

Increasing the number of impedance walls can effectively suppress resonances, so its effectiveness should be further studied. Fig. 7 shows

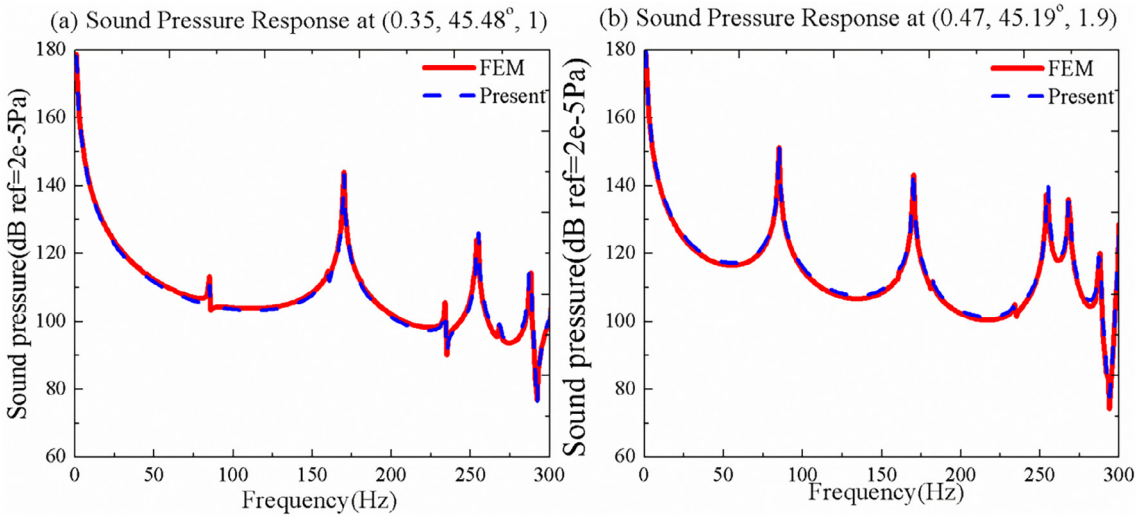

Fig. 5. Sound pressure responses inside air cavity with complex impedance $Z = \rho c_0(100\text{-}j)$ specified on the surface $z = h$ at: (a), (c) (0.35, 45.48°, 1) and (b), (d) (0.47, 45.19°, 1.9).

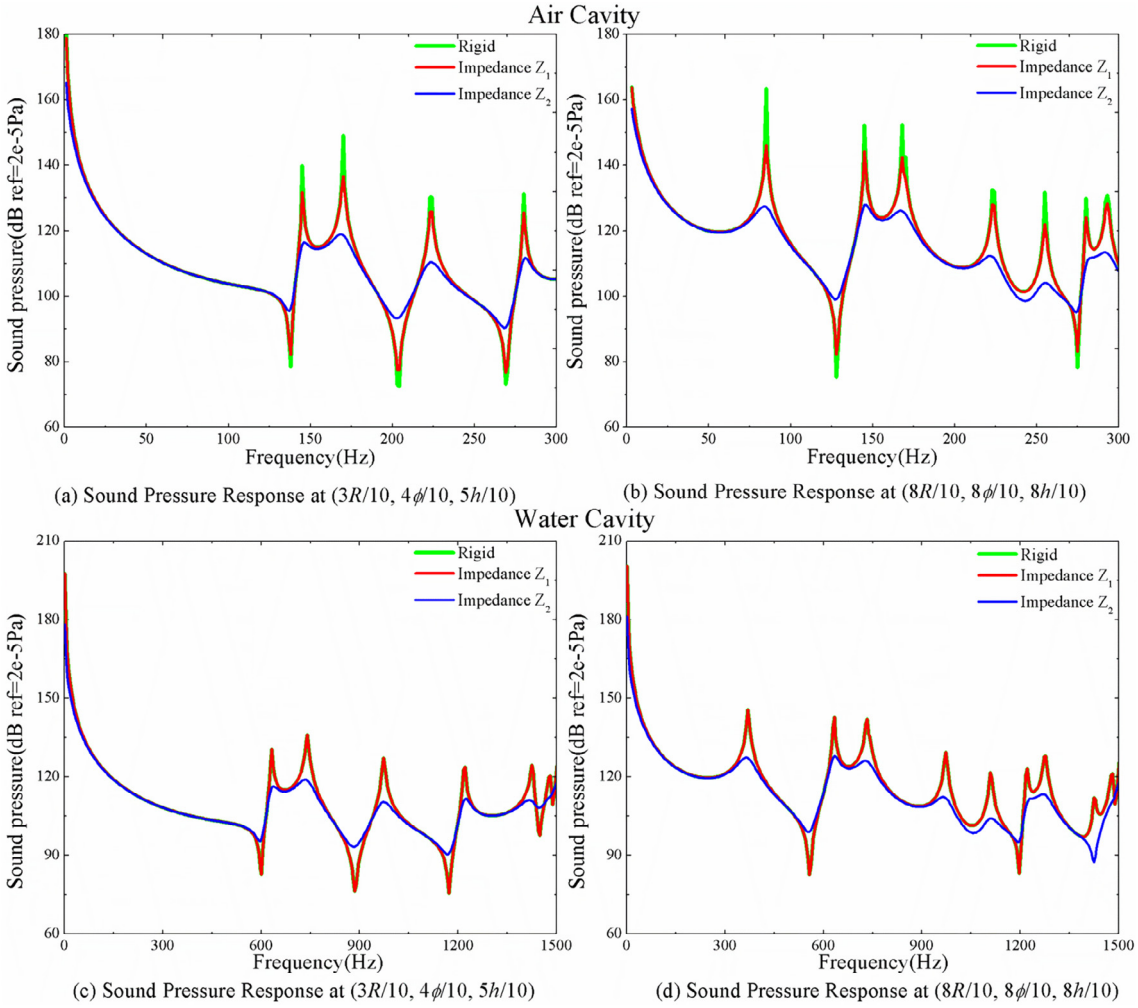

Fig. 6. Sound pressure responses with two impedance wall of $z = 0$ and $z = h$ inside the air cavity at: (a) ($3R/10$, $4\phi/10$, $5h/10$), (b) ($8R/10$, $8\phi/10$, $8h/10$), and the water cavity at: (c) ($3R/10$, $4\phi/10$, $5h/10$), (d) ($8R/10$, $8\phi/10$, $8h/10$).

the effect of the various number of impedance walls on the pressure response of the cavity. The geometrical dimensions of the cavity are $R_2/R_1 = 0.5$, $\phi = 90°$, and $h = 2$, separately. The modal damping coefficient ξ is 0.001 and the wall impedance value is $Z = \rho c_0(100\text{-}j)$. The point source is located at ($R/8$, $\phi/8$, $h/8$). The positions of the two observation points are at ($R/2$, $\phi/2$, $h/2$) and ($7R/8$, $7\phi/8$, $7h/8$). The sound pressure responses of the air cavity in the frequency range of 0–400 Hz are given in (a) and (b) of Fig. 7. Three different cases contain one impedance wall ($z = 0$), two impedance walls ($z = 0$ and $z = h$), and six impedance walls. Besides, the response of the water cavity in the frequency range of 0–1500 Hz is also given in (c) and (d) of Fig. 7. For sake of comparison, the sound pressure response of six surfaces with rigid boundary conditions is also investigated. From Fig. 7, we can find that it can effectively control the internal noise level under the resonance frequency by changing the acoustic impedance characteristics. The inhibitory effect is enhanced obviously when the number of impedance wall increases. The peak value of the pressure response is gradually obtuse. However, there is no change in the sound pressure response at the non-resonance frequency. Therefore, the use of impedance wall surfaces should be added as much as possible in engineering applications.

Conclusions

In this paper, a 3D Fourier series solution is extended to solve the acoustic characteristics for the annular segment cavity with various impedance boundary conditions. The sound pressure function can be expressed as a 3D Fourier cosine series and six supplementary polynomials which can ignore the influence of boundary conditions. Through the introduction of auxiliary polynomials, the discontinuous or jumping phenomenon of the displacement function on the boundaries can be overcome effectively. The formulations are based on energy approach and Rayleigh-Ritz technique to construct the dynamic system of the acoustic cavity.

Some important conclusions about acoustic characteristics of cavity are obtained, which are listed as follows:

(1) The annular segment cavity model established in this paper shows fast convergence and good accuracy.
(2) The effects of various geometric parameters and various medium inside the cavity on the natural frequencies of annular segment cavity are significant. It is helpful for the acoustic design of cavity by choosing suitable size and medium.
(3) The reduction of the impedance value or the increase of the number of the impedance wall can increase the dissipation of energy and effectively reduce the value of resonance peaks.

The above results suggest that it should be considered of the geometric parameters, medium and impedance wall synthetically in the process of design and noise reduction. At the same time, this study also establishes the foundation for the further research of rotary type cavity, such as conical cavity, spherical cavity, double curvature cavity and so on.

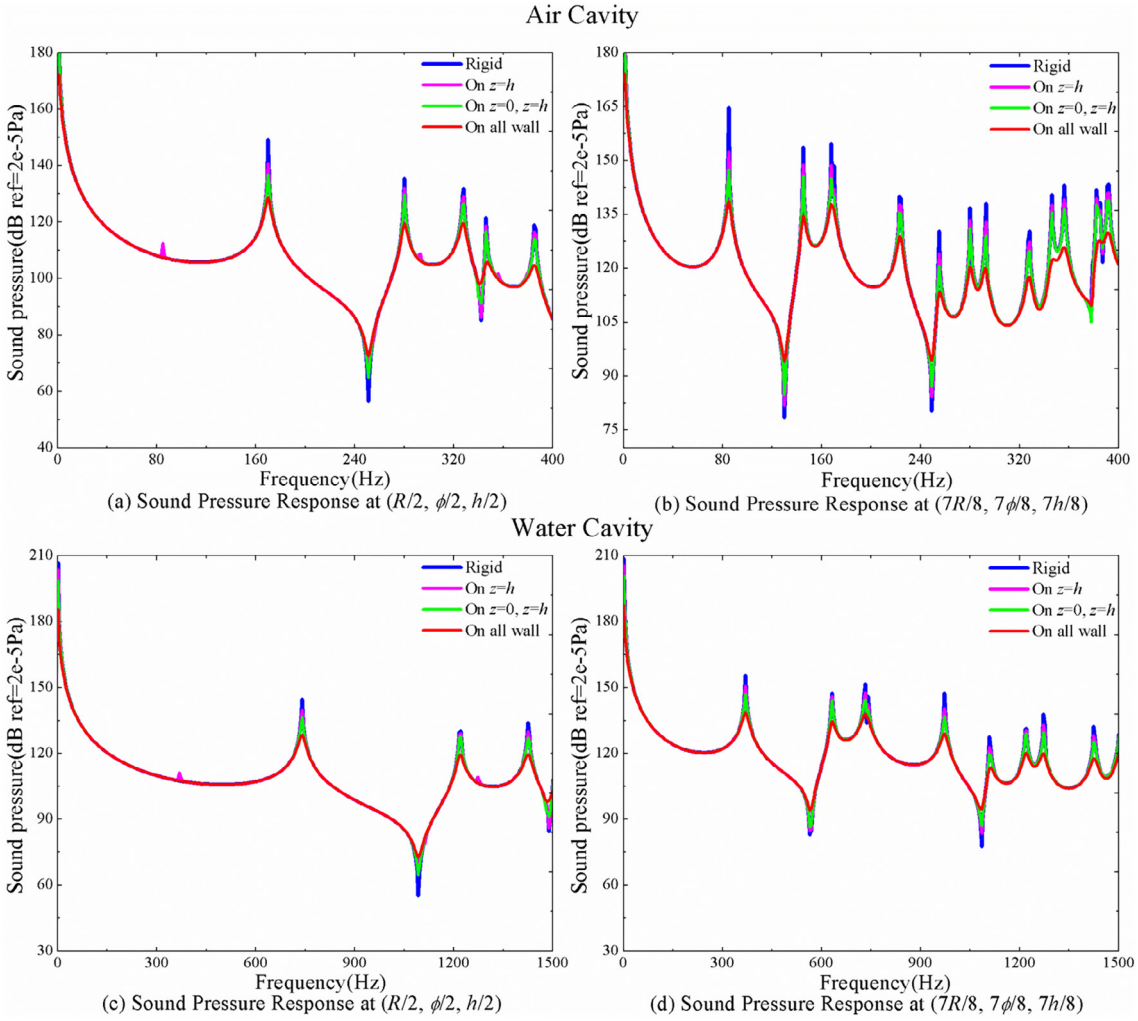

Fig. 7. Sound pressure responses with various impedance walls inside the air cavity at: (a) ($R/2$, $\phi/2$, $h/2$), (b) ($7R/8$, $7\phi/8$, $7h/8$), and the water cavity at: (c) ($R/2$, $\phi/2$, $h/2$), (d) ($7R/8$, $7\phi/8$, $7h/8$).

Acknowledgements

The authors would like to thank the anonymous reviewers for their very valuable comments. The authors also gratefully acknowledge the financial support from the National Natural Science Foundation of China (Grant Nos. 51705537), the Natural Science Foundation of Hunan Province of China (2018JJ3661) and the State Key Laboratory of High Performance Complex Manufacturing, Central South University, China (Grant No. ZZYJKT2018-11).

Appendix: Detailed expressions of matrices K, M, Z and F

The specific expressions of mass matrix **M** and stiffness matrix **K**, impedance matrix **Z** and force vector **F** can be written as follows:

$$\mathbf{K}_{1-1} = \frac{1}{\rho}\int_0^R\int_0^\phi\int_0^h \left\{\begin{array}{l}\left[\frac{\partial \mathbf{P}^{\Omega}(s,\theta,z)}{\partial s}\right]^2 + \left[\frac{\partial \mathbf{P}^{\Omega}(s,\theta,z)}{(s+R_2)\partial\theta}\right]^2 \\ + \left[\frac{\partial \mathbf{P}^{\Omega}(s,\theta,z)}{\partial z}\right]^2\end{array}\right\}(s+R_2)dsd\theta dz \tag{A.1}$$

$$\mathbf{K}_{1-f} = \frac{1}{\rho}\int_0^R\int_0^\phi\int_0^h \left\{\begin{array}{l}\left[\frac{\partial \mathbf{P}^{\Omega}(s,\theta,z)}{\partial s}\frac{\partial \mathbf{P}^{S}_{f-1}(s,\theta,z)}{\partial s}\right] \\ + \left[\frac{\partial \mathbf{P}^{\Omega}(s,\theta,z)}{(s+R_2)\partial\theta}\frac{\partial \mathbf{P}^{S}_{f-1}(s,\theta,z)}{(s+R_2)\partial\theta}\right] \\ + \left[\frac{\partial \mathbf{P}^{\Omega}(s,\theta,z)}{\partial z}\frac{\partial \mathbf{P}^{S}_{f-1}(s,\theta,z)}{\partial z}\right]\end{array}\right\}(s+R_2)dsd\theta dz \tag{A.2}$$

$$\mathbf{K}_{ef-f} = \frac{1}{\rho}\int_0^R\int_0^\phi\int_0^h \left\{ \begin{array}{l} \left[\frac{\partial \mathbf{P}^{\mathrm{S}}_{e-1}(s,\theta,z)}{\partial s}\frac{\partial \mathbf{P}^{\mathrm{S}}_{f-1}(s,\theta,z)}{\partial s}\right] \\ +\left[\frac{\partial \mathbf{P}^{\mathrm{S}}_{e-1}(s,\theta,z)}{(s+R_2)\partial\theta}\frac{\partial \mathbf{P}^{\mathrm{S}}_{f-1}(s,\theta,z)}{(s+R_2)\partial\theta}\right] \\ +\left[\frac{\partial \mathbf{P}^{\mathrm{S}}_{e-1}(s,\theta,z)}{\partial z}\frac{\partial \mathbf{P}^{\mathrm{S}}_{f-1}(s,\theta,z)}{\partial z}\right] \end{array} \right\}(s+R_2)dsd\theta dz \tag{A.3}$$

$$\mathbf{M}_{1-1} = \frac{1}{\rho c_0}\int_0^R\int_0^\phi\int_0^h \{[\mathbf{P}^{\Omega}(s,\theta,z)]^2(s+R_2)\}dsd\theta dz \tag{A.4}$$

$$\mathbf{M}_{1-f} = \frac{1}{\rho c_0}\int_0^R\int_0^\phi\int_0^h \{[\mathbf{P}^{\Omega}(s,\theta,z)\mathbf{P}^{\mathrm{S}}_{f-1}(s,\theta,z)](s+R_2)\}dsd\theta dz \tag{A.5}$$

$$\mathbf{M}_{e-f} = \frac{1}{\rho c_0}\int_0^R\int_0^\phi\int_0^h \{[\mathbf{P}^{\mathrm{S}}_{e-1}(s,\theta,z)\mathbf{P}^{\mathrm{S}}_{f-1}(s,\theta,z)](s+R_2)\}dsd\theta dz \tag{A.6}$$

$$\begin{aligned}\mathbf{Z}_{1-1} = {} & \frac{1}{jZ_1}\int_{S_1}[\mathbf{P}^{\Omega}(0,\theta,z)]^2dS_1|_{s=0} + \frac{1}{jZ_2}\int_{S_2}[\mathbf{P}^{\Omega}(R,\theta,z)]^2dS_2|_{s=R} + \frac{1}{jZ_3}\int_{S_3}[\mathbf{P}^{\Omega}(s,0,z)]^2dS_3|_{\theta=0} + \frac{1}{jZ_4}\int_{S_4}[\mathbf{P}^{\Omega}(s,\phi,z)]^2dS_4|_{\theta=\phi} \\ & + \frac{1}{jZ_5}\int_{S_5}[\mathbf{P}^{\Omega}(s,\theta,0)]^2dS_5|_{z=0} + \frac{1}{jZ_6}\int_{S_6}[\mathbf{P}^{\Omega}(s,\theta,h)]^2dS_6|_{z=h}\end{aligned} \tag{A.7}$$

$$\begin{aligned}\mathbf{Z}_{1-f} = {} & \frac{1}{jZ_1}\int_{S_1}[\mathbf{P}^{\Omega}(0,\theta,z)\mathbf{P}^{\mathrm{S}}_{f-1}(0,\theta,z)]dS_1|_{s=0} + \frac{1}{jZ_2}\int_{S_2}[\mathbf{P}^{\Omega}(R,\theta,z)\mathbf{P}^{\mathrm{S}}_{f-1}(R,\theta,z)]dS_2|_{s=R} + \frac{1}{jZ_3}\int_{S_3}[\mathbf{P}^{\Omega}(s,0,z)\mathbf{P}^{\mathrm{S}}_{f-1}(s,0,z)]dS_3|_{\theta=0} \\ & + \frac{1}{jZ_4}\int_{S_4}[\mathbf{P}^{\Omega}(s,\phi,z)\mathbf{P}^{\mathrm{S}}_{f-1}(s,\phi,z)]dS_4|_{\theta=\phi} + \frac{1}{jZ_5}\int_{S_5}[\mathbf{P}^{\Omega}(s,\theta,0)\mathbf{P}^{\mathrm{S}}_{f-1}(s,\theta,0)]dS_5|_{z=0} + \frac{1}{jZ_6}\int_{S_6}[\mathbf{P}^{\Omega}(s,\theta,h)\mathbf{P}^{\mathrm{S}}_{f-1}(s,\theta,h)]dS_6|_{z=h}\end{aligned} \tag{A.8}$$

$$\begin{aligned}\mathbf{Z}_{e-f} = {} & \frac{1}{jZ_1}\int_{S_1}[\mathbf{P}^{\mathrm{S}}_{e-1}(0,\theta,z)\mathbf{P}^{\mathrm{S}}_{f-1}(0,\theta,z)]dS_1|_{s=0} + \frac{1}{jZ_2}\int_{S_2}[\mathbf{P}^{\mathrm{S}}_{e-1}(R,\theta,z)\mathbf{P}^{\mathrm{S}}_{f-1}(R,\theta,z)]dS_2|_{s=R} + \frac{1}{jZ_3}\int_{S_3}[\mathbf{P}^{\mathrm{S}}_{e-1}(s,0,z)\mathbf{P}^{\mathrm{S}}_{f-1}(s,0,z)]dS_3|_{\theta=0} \\ & + \frac{1}{jZ_4}\int_{S_4}[\mathbf{P}^{\mathrm{S}}_{e-1}(s,\phi,z)\mathbf{P}^{\mathrm{S}}_{f-1}(s,\phi,z)]dS_4|_{\theta=\phi} + \frac{1}{jZ_5}\int_{S_5}[\mathbf{P}^{\mathrm{S}}_{e-1}(s,\theta,0)\mathbf{P}^{\mathrm{S}}_{f-1}(s,\theta,0)]dS_5|_{z=0} + \frac{1}{jZ_6}\int_{S_6}[\mathbf{P}^{\mathrm{S}}_{e-1}(s,\theta,h)\mathbf{P}^{\mathrm{S}}_{f-1}(s,\theta,h)]dS_6|_{z=h}\end{aligned} \tag{A.9}$$

$$\mathbf{F}_1 = \frac{4\pi A}{\rho}\int_0^R\int_0^\phi\int_0^h \{\mathbf{P}^{\Omega}(s,\theta,z)\delta(s-s_0)\delta(\theta-\theta_0)\delta(z-z_0)\}(s+R_2)dsd\theta dz \tag{A.10}$$

$$\mathbf{F}_e = \frac{4\pi A}{\rho}\int_0^R\int_0^\phi\int_0^h \{\mathbf{P}^{\mathrm{S}}_{e-1}(s,\theta,z)\delta(s-s_0)\delta(\theta-\theta_0)\delta(z-z_0)\}(s+R_2)dsd\theta dz \tag{A.11}$$

where $e = f = 2, 3, 4, 5, 6, 7$.

References

[1] Koch W. Acoustic resonances in rectangular open cavities. AIAA J 2005;43:2342–9.
[2] Huang Z, Jiang W. Analysis of source models for two-dimensional acoustic systems using the transfer matrix method. J Sound Vib 2007;306:215–26.
[3] Dhandole S, Modak S. A constrained optimization based method for acoustic finite element model updating of cavities using pressure response. Appl Math Model 2012;36:399–413.
[4] González L, Cobo P, Theofilis V, Valero E. Acoustic resonances in 2d open cavities. Acta Acustica United Acustica 2013;99:572–81.
[5] Aktas MK, Farouk B. Numerical simulation of acoustic streaming generated by finite-amplitude resonant oscillations in an enclosure. J Acoust Soc Am 2004;116:2822–31.
[6] Huang Z, Jiang W. An effective method calculating acoustic Green's function for closed rectangular cavity using the Ewald's summation technique. Acta Acustica United Acustica 2007;93:853–6.
[7] Larbi W, Deü JF, Ohayon R. A new finite element formulation for internal acoustic problems with dissipative walls. Int J Numer Methods Eng 2006;68:381–99.
[8] Pàmies T, Romeu J, Genescà M, Balastegui A. Sound radiation from an aperture in a rectangular enclosure under low modal conditions. J Acoust Soc Am 2011;130:239–48.
[9] Li Y, Cheng L. Modifications of acoustic modes and coupling due to a leaning wall in a rectangular cavity. J Acoust Soc Am 2004;116:3312–8.
[10] Li Y, Cheng L. Vibro-acoustic analysis of a rectangular-like cavity with a tilted wall. Appl Acoust 2007;68:739–51.
[11] Petyt M, Lea J, Koopmann G. A finite element method for determining the acoustic modes of irregular shaped cavities. J Sound Vib 1976;45:495–502.
[12] Petyt M, Koopmann G, Pinnington R. The acoustic modes of a rectangular cavity containing a rigid, incomplete partition. J Sound Vib 1977;53:71–82.
[13] Pan J, Elliott S, Baek K-H. Analysis of low frequency acoustic response in a damped rectangular enclosure. J Sound Vib 1999;223:543–66.
[14] Nabavi M, Siddiqui K, Dargahi J. Analysis of regular and irregular acoustic streaming patterns in a rectangular enclosure. Wave Motion 2009;46:312–22.
[15] Guha Niyogi A, Laha M, Sinha P. A coupled FE-BE analysis of acoustic cavities confined inside laminated composite enclosures. Aircraft Eng Aerosp Technol 2000;72:345–57.
[16] Du JT, Li WL, Liu ZG, Xu HA, Ji ZL. Acoustic analysis of a rectangular cavity with general impedance boundary conditions. J Acoust Soc Am 2011;130:807–17.
[17] Shi SX, Jin GY, Liu ZG. Vibro-acoustic behaviors of an elastically restrained double-panel structure with an acoustic cavity of arbitrary boundary impedance. Appl Acoust 2014;76:431–44.
[18] Xie X, Zheng H, Qu Y. A variational formulation for vibro-acoustic analysis of a panel backed by an irregularly-bounded cavity. J Sound Vib 2016;373:147–63.
[19] Xie X, Yang H, Zheng H. A weak formulation for interior acoustic analysis of enclosures with inclined walls and impedance boundary. Wave Motion 2016;65:175–86.
[20] Bouillard P, Lacroix V, De Bel E. A wave-oriented meshless formulation for acoustical and vibro-acoustical applications. Wave Motion 2004;39:295–305.
[21] Bouzouane B, Ghorbel A, Akrout A, Abdennadher M, Boukharouba T, Haddar M. Ultra-thin films effects on vibro-acoustic behaviour of laminated plate including a viscoelastic core. Appl Acoust 2018.
[22] Zhang H, Shi D, Zha S, Wang Q. Vibro-acoustic analysis of the thin laminated rectangular plate-cavity coupling system. Compos Struct 2018;189:570–85.
[23] Zhang H, Shi D, Zha S, Wang Q. Parameterization study on the moderately thick laminated rectangular plate-cavity coupling system with uniform or non-uniform boundary conditions. Compos Struct 2018;194:537–54.
[24] Shi S, Su Z, Jin G, Liu Z. Vibro-acoustic modeling and analysis of a coupled acoustic system comprising a partially opened cavity coupled with a flexible plate. Mech Syst Sig Process 2018;98:324–43.
[25] Shi S, Jin G, Xiao B, Liu Z. Acoustic modeling and eigenanalysis of coupled rooms with a transparent coupling aperture of variable size. J Sound Vib 2018;419:352–66.
[26] Laulagnet B, Guyader J. Modal analysis of a shell's acoustic radiation in light and heavy fluids. J Sound Vib 1989;131:397–415.
[27] Gardonio P, Ferguson N, Fahy F. A modal expansion analysis of noise transmission through circular cylindrical shell structures with blocking masses. J Sound Vib 2001;244:259–97.

[28] Yang D, Zhang R, Shi S, He T. Sound radiation from a finite cylindrical shell with an irregular-shaped acoustic enclosure. J Acoust Soc Am 2017;142. 2687–2687.
[29] Shi J, Zhang X, Chen R, Zhang G. Acoustic radiation force of a solid elastic sphere immersed in a cylindrical cavity filled with ideal fluid. Wave Motion 2018;80:37–46.
[30] Wang Q, Cui X, Qin B, Liang Q. Vibration analysis of the functionally graded carbon nanotube reinforced composite shallow shells with arbitrary boundary conditions. Compos Struct 2017;182:364–79.
[31] Wang Q, Cui X, Qin B, Liang Q, Tang J. A semi-analytical method for vibration analysis of functionally graded (FG) sandwich doubly-curved panels and shells of revolution. Int J Mech Sci 2017;134:479–99.
[32] Wang Q, Qin B, Shi D, Liang Q. A semi-analytical method for vibration analysis of functionally graded carbon nanotube reinforced composite doubly-curved panels and shells of revolution. Compos Struct 2017;174:87–109.
[33] Zhou Y, Wang Q, Shi D, Liang Q, Zhang Z. Exact solutions for the free in-plane vibrations of rectangular plates with arbitrary boundary conditions. Int J Mech Sci 2017;130:1–10.
[34] Choe K, Tang J, Shui C, Wang A, Wang Q. Free vibration analysis of coupled functionally graded (FG) doubly-curved revolution shell structures with general boundary conditions. Compos Struct 2018;194:413–32.
[35] Choe K, Wang Q, Tang J. C. shui, Vibration analysis for coupled composite laminated axis-symmetric doubly-curved revolution shell structures by unified Jacobi-Ritz method. Compos Struct 2018;194:136–57.
[36] Guan X, Tang J, Shi D, Shuai C, Wang Q. A semi-analytical method for transverse vibration of sector-like thin plate with simply supported radial edges. Appl Math Model 2018;60:48–63.
[37] Guan X, Tang J, Wang Q, Shuai C. Application of the differential quadrature finite element method to free vibration of elastically restrained plate with irregular geometries. Eng Anal Boundary Elem 2018;90:1–16.
[38] Guo J, Shi D, Wang Q, Tang J, Shuai C. Dynamic analysis of laminated doubly-curved shells with general boundary conditions by means of a domain decomposition method. Int J Mech Sci 2018;138–139:159–86.
[39] Wang Q, Choe K, Shi D, Sin K. Vibration analysis of the coupled doubly-curved revolution shell structures by using Jacobi-Ritz method. Int J Mech Sci 2018;135:517–31.
[40] Wang Q, Shao D, Qin B. A simple first-order shear deformation shell theory for vibration analysis of composite laminated open cylindrical shells with general boundary conditions. Compos Struct 2018;184:211–32.
[41] Zhong R, Wang Q, Tang J, Shuai C, Qin B. Vibration analysis of functionally graded carbon nanotube reinforced composites (FG-CNTRC) circular, annular and sector plates. Compos Struct 2018;194:49–67.
[42] Bistafa SR, Morrissey JW. Numerical solutions of the acoustic eigenvalue equation in the rectangular room with arbitrary (uniform) wall impedances. J Sound Vib 2003;263:205–18.
[43] Naka Y, Oberai AA, Shinn-Cunningham BG. Acoustic eigenvalues of rectangular rooms with arbitrary wall impedances using the interval Newton/ generalized bi-section method. J Acoust Soc Am 2005;118:3662–71.
[44] Crighton D, Dowling A, Williams JF, Heckl M, Leppington F. Modern methods in analytical acoustics. J Fluid Mech 1996;318:410–2.
[45] Pan J. A third note on the prediction of sound intensity. J Acoust Soc Am 1999;105:560–2.
[46] Ginsberg JH. Mechanical and structural vibration: theory and applications. Georgia Institute of Technology, John Wiley & Sons, Inc; 2001.
[47] Blevins R. Formulas for natural frequency and mode shape. New York: Kreiger Publ. Comp.; 1979.
[48] Johnson M, Elliott S, Baek K, Garcia-Bonito J. An equivalent source technique for calculating the sound field inside an enclosure containing scattering objects. J Acoust Soc America 1998;104:1221–31.